Morphing the He–OCS intermolecular potential

Joanna M. M. Howson and Jeremy M. Hutson

Citation: The Journal of Chemical Physics **115**, 5059 (2001); doi: 10.1063/1.1394940
View online: http://dx.doi.org/10.1063/1.1394940
View Table of Contents: http://scitation.aip.org/content/aip/journal/jcp/115/11?ver=pdfcov
Published by the AIP Publishing

Morphing the He–OCS intermolecular potential

Joanna M. M. Howson and Jeremy M. Hutson
Department of Chemistry, University of Durham, South Road, Durham, DH1 3LE, England

(Received 7 August 2000; accepted 27 June 2001)

A potential energy surface for He–OCS that agrees with experimental rotational spectra to within 1 MHz is presented. The potential was first calculated at a grid defined in prolate spheroidal coordinates, which give stabler interpolations than Jacobi coordinates. Coupled cluster calculations at the CCSD(T) level were carried out with an aug-cc-pVTZ basis set. The potential was then morphed, a procedure that scales the energy and the intermolecular distance in a coordinate-dependent way. The parameters of the function used for morphing were determined by a least-squares fit to the experimental data. The global minimum of the recommended potential, at -50.2 cm^{-1}, is 4.8 cm^{-1} deeper than the unscaled potential of Higgins and Klemperer [J. Chem. Phys. **110**, 1383 (1999)]. The morphing procedure increases the well depth by more at the sulfur end than at the oxygen end. © *2001 American Institute of Physics.* [DOI: 10.1063/1.1394940]

I. INTRODUCTION

There is considerable current interest in the properties and behavior of molecules in liquid helium droplets.[1] Such droplets have many novel properties, and allow the preparation of a variety of unusual species that are inaccessible in other experiments. Both small molecules such as SF_6 (Ref. 2) and OCS (Ref. 3) and large molecules such as tryptophan[4] have been observed in helium droplets. The droplets also provide a novel environment for studying atomic[5] and molecular[6] clusters and chemical reactions.[7]

In recent experiments, Grebenev *et al.*[3,8] measured the rotationally resolved infrared spectrum of the OCS molecule in helium droplets. The molecule was found to have a rotational constant of 0.0732 cm^{-1} in the droplet environment, compared to the value of 0.2029 cm^{-1} in the gas phase. Many other molecules have also been found to have reduced rotational constants in the droplet environment,[9] though some, like HCN, retain almost their full gas-phase values.[10] This observation has sparked a considerable amount of theoretical work.[11,12]

Any proper understanding of the behavior of molecules in droplets requires knowledge of the He–molecule interaction potential. For He–OCS, Higgins and Klemperer[13] have measured rotational spectra and interpreted them in terms of an *ab initio* potential. Other experimental work on He–OCS has included the measurement of diffusion and thermal diffusion factors,[14] rotationally inelastic integral cross sections[15] and total differential cross sections (although the last were not resolved into elastic and inelastic contributions).[16]

There have also been a number of *ab initio* studies of He–OCS. Danielson, Mcleod and Keil[17] carried out Hartree–Fock calculations of the repulsive interaction at a variety of geometries and added a dispersion term. Sadlej and Edwards[18] carried out geometry optimizations at the MP4 (fourth-order Møller–Plesset) level and found two linear and one T-shaped potential minima. The most thorough study so far was that performed by Higgins and Klemperer (HK),[13] who carried out counterpoise-corrected MP4 calculations on an irregular grid of 98 points, at 13 different angles, with 2.5 Å$\leqslant R \leqslant$10.0 Å. They used a basis set that included ''bond-centered'' functions, which have been found to be effective at speeding convergence of the dispersion energy. Higgins and Klemperer then fitted a functional form to the data at each angular cut in order to generate a regular grid of 175 points, on the range 2.5 Å$\leqslant R \leqslant$20.0 Å. By putting a bicubic spline through the points on this grid they obtained a potential surface with three minima. In its unmodified form, this potential gave rotational constants for He–OCS that were significantly below the experimental values. However, based on experience with other systems Higgins and Klemperer proposed increasing the well depth by 10% and reducing the intermolecular distance by 0.05 Å. This gave improved agreement with the centrifugal distortion constants and the rotational constants.

Meuwly and Hutson[19] have recently developed a ''morphing'' procedure which allows an *ab initio* potential to be adjusted to fit experimental data in a systematic way. In this approach, angle-dependent energy and distance scalings are introduced, and their parameters determined by least-squares fitting to experimental data. The procedure retains the general shape of the *ab initio* potential, but allows such things as barrier heights and the absolute and relative depths and distances of potential minima to be adjusted. It has antecedents in the work of Bowman and co-workers,[20–23] who also introduced coordinate-dependent scaling functions to refine *ab initio* potentials. Meuwly and Hutson carried out a systematic study of morphing for Ne–HF, and showed that the final potential obtained from morphing was remarkably insensitive to the quality of the *ab initio* potential used as a starting point.

In this work we apply the morphing procedure to He–OCS.

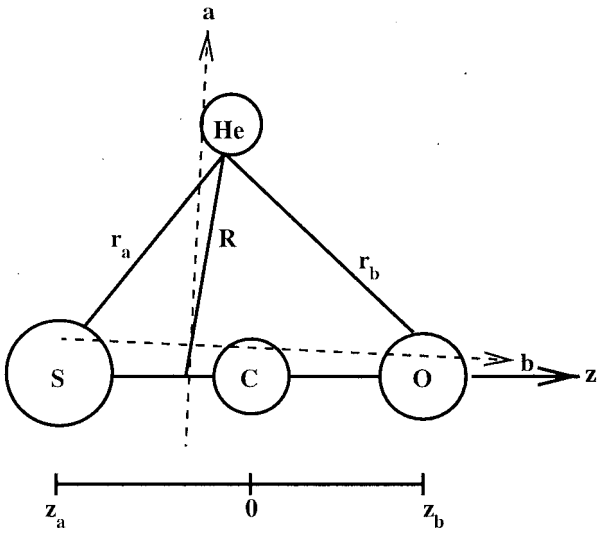

FIG. 1. The He–OCS inertial axes and distances used to define prolate spheroidal coordinates.

II. THEORETICAL METHODS

A. Coordinate system

The potential energy surfaces for atom–molecule systems are usually represented in Jacobi coordinates. However, we have found that, for interactions between atoms and linear molecules, prolate spheroidal coordinates allow more accurate interpolation and more economical grid choices than Jacobi coordinates.[24] We therefore adopt prolate spheroidal coordinates (elliptical coordinates) in the present work.

In two dimensions, a set of elliptical coordinates is defined as shown in Fig. 1, in terms of a baseline that runs between foci at z_a and z_b on the z axis, and the distances r_a and r_b from the foci to a family of confocal ellipses and hyperbolas. The elliptical coordinates ξ and η are given by

$$\xi=\frac{r_a+r_b}{z_a+z_b} \quad \text{and} \quad \eta=\frac{r_a-r_b}{z_a+z_b}, \tag{1}$$

and are defined with ranges

$$1\leqslant\xi\leqslant\infty \quad \text{and} \quad -1\leqslant\eta\leqslant 1. \tag{2}$$

ξ is a distancelike (but dimensionless) coordinate and η is an anglelike coordinate. Prolate spheroidal coordinates are obtained from elliptical coordinates simply by rotating the ellipse about its major axis and introducing an azimuthal angle ϕ; since an atom–linear molecule potential is cylindrically symmetrical, we may speak interchangeably of elliptical or prolate spheroidal coordinates.

In the present work, we used a baseline that runs between the oxygen and sulfur nuclei. (Note that this is not quite the same baseline as recommended in Ref. 24: the calculations described here were completed before those recommendations were finalized.) The helium–sulfur distance corresponds to r_a and the helium–oxygen distance to r_b. Thus, when $\eta=-1.0$, helium is next to sulfur and when $\eta=1.0$ it is next to oxygen.

The work of Higgins and Klemperer was in Jacobi coordinates. In the present work, the Jacobi system is set up with the He atom at the oxygen end for $\theta=0$ and at the sulfur end for $\theta=180°$. This is the opposite convention to that used by Higgins and Klemperer.[13]

TABLE I. Comparison of He–OCS interaction energies at a single point for aug-cc-pVTZ and aug-cc-pVQZ basis sets. The energies are corrected for basis set superposition error. Calculations were carried out using GAUSSIAN 94, running on a single processor (195 MHz R10000) of a Silicon Graphics Origin 2000.

Basis set	Method	Energy	CPU time per point
aug-cc-pVTZ	CCSD(T)	-18.15 cm^{-1}	42 hrs 36 mins
aug-cc-pVTZ	CCSD(T,FC)	-18.08 cm^{-1}	10 hrs 45 mins
aug-cc-pVQZ	CCSD(T)	-21.21 cm^{-1}	2 weeks
aug-cc-pVQZ	CCSD(T,FC)	-21.16 cm^{-1}	6 days

B. The unmorphed potential: *Ab initio* calculations

We chose to carry out *ab initio* calculations on a product grid of 246 points, made up of 13 Gauss–Legendre quadrature points in η and 19 equally spaced points in ξ. The range of interest, $2.3\leqslant\xi\leqslant 4.8$, was established from the HK potential. We used CCSD(T) calculations (coupled cluster calculations including single, double, and noniterative triple excitations), which have been shown to reproduce the potential shape faithfully for Ne–HF.[19] As the number of points required was large and the CPU time available was limited, the size of basis set that we could afford was restricted. The basis set convergence at a single point and the corresponding CPU times are shown in Table I for Dunning's correlation-consistent aug-cc-pVTZ and aug-cc-pVQZ basis sets,[25–28] for both full correlation and frozen core methods. The aug-cc-pVTZ basis was found to provide a good compromise between CPU time and accuracy. The difference in counterpoise-corrected interaction energy between the frozen core and full correlation CCSD(T) methods at the single point calculated was 0.07 cm^{-1} while the saving in CPU time was almost a factor of 4. Hence, frozen core CCSD(T) was employed for calculations on the full grid of 246 points.

The full counterpoise method of Boys and Bernardi[29] was used to correct for basis set superposition error. All the *ab initio* computations were carried out with GAUSSIAN 94.[30] The OC and CS bond lengths were held fixed at 1.16 Å and 1.56 Å, respectively.

At each cut in ξ the potential was expanded in Legendre polynomials,

$$V(\xi,\eta)=\sum_{\lambda} V_{\lambda}(\xi)P_{\lambda}(\eta). \tag{3}$$

The reproducing kernel Hilbert space (RKHS) interpolation scheme developed by Ho and Rabitz[31] was then used to interpolate between the points in ξ for each λ. The resulting potential is plotted in Fig. 2.

The raw (unmorphed) potential has a global minimum of depth 43.27 cm^{-1} at $\theta=69.7°$, $R=3.40$ Å, and two linear minima at each end of the OCS molecule. The minimum at the oxygen end is 25.21 cm^{-1} deep with $R=4.82$ Å. This is shallower than the minimum at the sulfur end, which is 27.90 cm^{-1} deep with $R=4.52$ Å. The two linear minima are sepa-

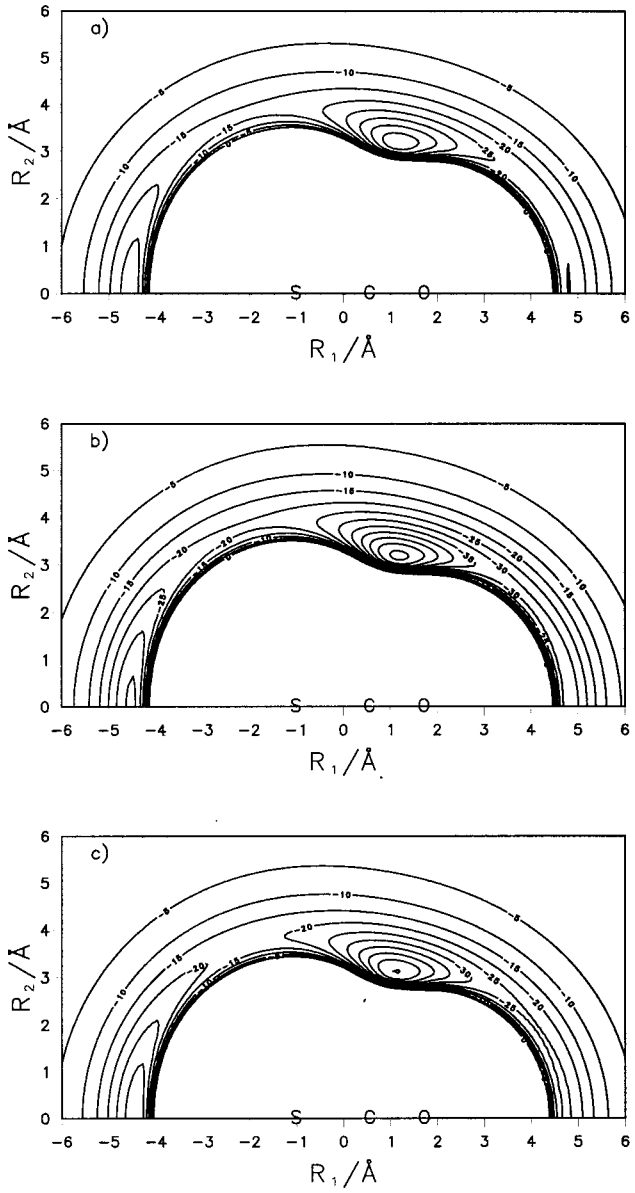

FIG. 2. Contour plots of He–OCS potentials. (a) The unmorphed potential obtained from CCSD(T) calculations with aug-cc-pVTZ basis sets; (b) the isotropically morphed (two-parameter) potential; (c) the anisotropically morphed (four-parameter) potential. Contours are labeled in cm^{-1}.

rated from the global minimum by transition states found at $(R/\text{Å},\ \theta/°)=(4.33,119.1)$ and $(4.55,29.4)$, with energies -15.81 cm^{-1} and -23.84 cm^{-1}, respectively. Hence the potential in the region of the oxygen atom is quite flat. Our results agree qualitatively with the HK potential, which has a global minimum 45.39 cm^{-1} deep and two secondary minima at the linear configurations.

III. EXPERIMENTAL DATA

Higgins and Klemperer[13] measured 10 rotational transitions in the vibrational ground state of the He–OCS complex, which are shown schematically in Fig. 3. These transition frequencies were used for the least-squares fit with uncertainties of ± 1 MHz. These uncertainties essentially

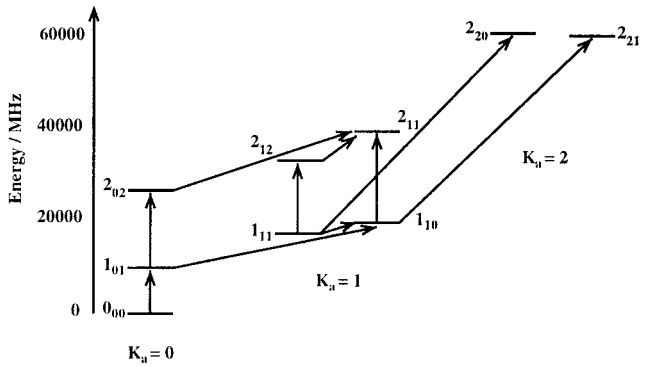

FIG. 3. Energy level diagram showing the rotational transitions measured by Higgins and Klemperer (Ref. 13). Energy levels are labeled $J_{K_aK_c}$.

correspond to the desired agreement between experiment and theory; they are considerably larger than the actual experimental uncertainties.

The quantities included in the least-squares fits were the actual transition frequencies. However, when comparing different potentials it is conceptually useful to consider the *A*, *B*, and *C* rotational constants and an appropriate set of centrifugal distortion constants calculated from the different potentials. Spectroscopic constants such as these tell us about specific features of the potential, which raw transition frequencies do not, so that physical insight can be gained. Although in this work we decided that there was little advantage in fitting to the constants directly, they were found to be helpful in assessing the discrepancies between observed and calculated frequencies and understanding how they relate to the shape of the potential.

Experimentally, spectroscopic constants are usually obtained by least-squares fitting to an effective Hamiltonian; for He–OCS, Higgins and Klemperer used the Watson A-reduced Hamiltonian. Calculated spectroscopic constants can in principle be obtained by the same approach, but the procedure is cumbersome, because it involves calculations for several different values of the total angular momentum *J* and an extra level of least-squares fitting. It is more convenient to obtain quantities *approximately* proportional to the rotational and centrifugal distortion constants from combinations of low-*J* level energies or transition frequencies. These approximate constants roll up the effects of higher-order centrifugal distortion into the low-order constants, but still allow a direct comparison between experiment and theory because the approximations are identical for the two cases.

He–OCS is a prolate near-symmetric rotor molecule: the inertial axes for the system are shown in Fig. 1. In the following, level energies are labeled in terms of asymmetric top quantum numbers, $J_{K_aK_c}$.

The combination of level energies $1_{10}+1_{11}-1_{01}$ is approximately equal to $2A$ (neglecting centrifugal distortion). Using combinations of the transition frequencies, $(1_{10} \leftarrow 1_{11})$, $(1_{01} \leftarrow 0_{00})$, and $(1_{10} \leftarrow 1_{01})$, measured by Higgins and Klemperer, gives 26 321.613 MHz for this quantity (which will be referred to simply as $2A$ from now on). It may be noted that, if He–OCS was a rigid molecule with the He atom at $\theta=90°$, *A* would be the same as the OCS rota-

tional constant, $b_{OCS}=6081.49$ MHz. In reality, A is substantially larger than b_{OCS}, because of the effects of wide-amplitude motion and because the equilibrium geometry is not $\theta=90°$.

The combination of level energies $1_{10}-1_{11}+1_{01}$ is approximately $2B$. A different combination of the same three transition frequencies as for $2A$ gives an experimental value of 10 962.705 MHz for this quantity. The B rotational constant gives information principally on the intermolecular distance, and hence on R_{min}.

The level energy combination $1_{11}-1_{10}+1_{01}$ is approximately $2C$. Yet another combination of the same three transition frequencies gives 7360.919 MHz for $2C$. The C rotational constant gives information on the radial and angular amplitude of motion.

The centrifugal distortion constants can be approximated using level energies and transition frequencies for $J\leqslant 2$. For example, the centrifugal distortion constant D_J gives information on the radial curvature of the potential in the region of the minimum. The combination of level energies

$$(2_{02}+(2_{20}-2_{21})-1_{01})-2\times(1_{01}-0_{00}),$$

gives a quantity approximately equal to $-24D_J$ for He–OCS. Using transition frequencies measured by Higgins and Klemperer gives and experimental value of -22.576 MHz for this quantity; it will be referred to as $-24D_J$ for simplicity, even though it actually contains contributions from higher-order centrifugal distortion.

The quantity

$$(2_{11}+\tfrac{1}{2}(2_{12}-2_{11})-(2_{02}+(2_{20}-2_{21})))$$
$$-(\tfrac{1}{2}(1_{11}+1_{10})-1_{01}), \quad (4)$$

is approximately equal to $-4D_{JK}$. It gives an indication of the way the angular wave function changes as the molecule is stretched by centrifugal distortion, and hence on the degree of angular-radial coupling. distortion. Using the measured transition frequencies gives an experimental value of -5.594 MHz for this quantity, which will be referred to as $-4D_{JK}$ for simplicity.

Finally, the quantity

$$-516.850\ \text{MHz}=(2_{21}-\tfrac{1}{2}(2_{11}+2_{12}))$$
$$-3[\tfrac{1}{2}(2_{11}+2_{12})-(2_{02}+(2_{20}-2_{21}))]$$

is approximately equal to $-12D_K$. This gives an indication of how the bending amplitude of motion alters as the molecule is stretched by centrifugal distortion.

IV. BOUND STATE CALCULATIONS

In order to compare the rotational levels for this potential with those from experiment, the close-coupling equations[32] were constructed and solved using the BOUND program.[33] The bound states reported here are for the isotopic species ^{4}He–^{16}O^{12}C^{32}S, as this is the species that was studied experimentally. The rotational constant b_{OCS} was taken to be 0.202 85 74 cm^{-1} for $v_{OCS}=0$,[34] with basis functions up to $j=30$ included in the calculations. The reduced mass of the complex was taken as 3.752 159 m_u and the coupled equations propagated from $R_{min}=2.2$ Å to $R_{max}=6.5$ Å. This gives convergence to better than 1×10^{-4} MHz for the eigenvalues and considerably better for the rotational constants.

The BOUND program operates in Jacobi coordinates, whereas the potentials used in this work are specified in prolate spheroidal coordinates. It is however unnecessary to alter BOUND itself to deal with prolate spheroidal coordinates; instead, when the potential routine is called by BOUND, it calculates the equivalent position in prolate spheroidal coordinates before evaluating the potential at that point.

V. THE MORPHING PROCEDURE

The functional form used to morph the surface is the same as that used by Meuwly and Hutson,[19] except the angle dependence is handled here in terms of the spheroidal coordinate η instead of the Jacobi cos θ. The morphing transformation is

$$V_{morph}(\xi,\eta)=v(\eta)V_{orig}(\rho(\eta)\cdot\xi,\eta), \quad (4)$$

where

$$\rho(\eta)=\sum_\lambda \rho_\lambda P_\lambda(\eta),$$
$$v(\eta)=\sum_\lambda v_\lambda P_\lambda(\eta). \quad (5)$$

The parameters, v_λ and ρ_λ, are determined by a least-squares fit to the experimental data. The scaling is applied to first to the radial coordinate and then to the energy. The radial scaling allows the distance at which the interaction energy passes through zero to be different for the morphed and unmorphed surfaces.

The first terms in the expansions of $v(\eta)$ and $\rho(\eta)$ are isotropic scaling factors. They can be used to adjust the well depth and the corresponding radial distance. The higher order terms in $v(\eta)$ and $\rho(\eta)$ introduce anisotropic scaling. The second term in $v(\eta)$ allows the minimum energy at the carbon end of OCS to be adjusted relative to the energy at the oxygen end.

The morphing function allows the surface to be bent and stretched by small amounts to reproduce the experimental data, but the general shape of the *ab initio* potential is retained. The amount of morphing needed, measured by the size and number of morphing parameters required to obtain agreement with experiment, depends on the quality of the initial surface.

A. The morphed potentials

The least-squares fits to the spectroscopic data were carried out using the I–NoLLS program.[35,36] I–NoLLS is an interactive nonlinear least-squares fitting program which allows the user to apply physical insight to guide the progress of a fit. It is particularly useful for highly nonlinear fits with strongly correlated parameters, for which ''black box'' fitting routines often wander irretrievably into unphysical regions of parameter space.

TABLE II. The morphing parameters of the isotropically morphed (two-parameter) potential and the anisotropically morphed (four-parameter) potential obtained in the present work. The 95% confidence limits are given in parentheses.

Parameter	Isotropic morphing	Anisotropic morphing
v_0	1.302 242(0.316 130)	1.163 040(0.037 658)
v_1	0.0	−0.087 796(0.033 104)
v_2	0.0	−0.044 405(0.041 718)
ρ_0	1.005 704(0.009008)	1.019 728(0.000 647)

CCSD(T) computations with a finite basis set usually underestimate the dispersion energy. Consequently, they underestimate intermolecular well depths and overestimate intermolecular distances. It is thus reasonable to expect that at least isotropic scaling in the energy and the distance will be required. Accordingly, we began by performing an isotropic two-parameter morphing, with parameters v_0 and ρ_0 only. The best-fit parameters are given in Table II and the potential is plotted in the central panel of Fig. 2. The resulting fit to the experimental data is shown in Table III: the agreement with experiment is much improved, overall, but has actually deteriorated for the transition out of the $J_{K_aK_c}=2_{02}$ state. In addition, the $1_{10}\leftarrow 1_{11}$ and $2_{11}\leftarrow 2_{12}$ asymmetry splittings are poor. This is manifested as large errors in the centrifugal distortion constants, particularly in D_{JK}. We can conclude that the isotropic morphing provides insufficient flexibility to model the potential anisotropy properly.

We next investigated anisotropic morphing. With the addition of v_1 and v_2, we found that we could obtain rotational transitions that agree with experiment to within 1 MHz, as shown in Table III. Also listed in Table III are the rotational and centrifugal distortion constants. Very good agreement is obtained with the rotational constants, which demonstrates that the position of the global minimum is good. The largest error occurs for D_{JK}. Although fits were also performed that included the addition of v_1 or v_2 only, the fits were poorer and the resulting potentials were a little unphysical with either an excessively deep or an excessively shallow sulfur end. D_{JK} was found to be particularly sensitive to the depth of the potential at the sulfur end and so served as a good aid when deciding upon the best fit.

TABLE III. Comparison of experimental and calculated rotational transition frequencies (in MHz) for He–OCS.

Transition $J_{K_aK_c}\leftarrow J_{K_aK_c}$	Experiment	Unmorphed CCSD(T)	Isotropic morphed	Anisotropic morphed	Unscaled HK
$1_{10}\leftarrow 1_{11}$	1801.0	1806.3	1741.6	1801.1	1835.8
$1_{01}\leftarrow 0_{00}$	9161.8	8947.1	9067.7	9161.7	9053.5
$1_{10}\leftarrow 1_{01}$	9480.3	9445.9	9502.4	9479.7	9201.8
$2_{11}\leftarrow 2_{12}$	5386.5	5388.8	5211.8	5386.2	5485.6
$2_{11}\leftarrow 2_{02}$	11 539.3	11 518.8	11 488.6	11 540.0	11 317.9
$2_{12}\leftarrow 1_{11}$	16 502.6	16 076.1	16 378.5	16 503.4	16 252.5
$2_{02}\leftarrow 1_{01}$	18 029.3	17 585.7	17 862.5	18 028.3	17 786.3
$2_{11}\leftarrow 1_{10}$	20 088.3	19 658.6	19 848.7	20 088.5	19 902.4
$2_{21}\leftarrow 1_{10}$	42 601.1	41 561.2	42 683.9	42 601.0	41 284.3
$2_{20}\leftarrow 1_{11}$	44 673.7	43 634.8	44 680.4	44 673.9	43 409.8
$2A$	26 321.6	26 032.5	26 331.0	26 320.1	25 621.3
$2B$	10 962.7	10 753.4	10 809.3	10 962.8	10 889.2
$2C$	7360.9	7140.7	7326.1	7360.7	7217.7
$24D_J$	22.6	41.2	18.1	23.3	30.9
$4D_{JK}$	5.6	−14.4	3.8	4.2	−1.3
$12D_K$	516.9	1074.5	442.5	519.5	731.0

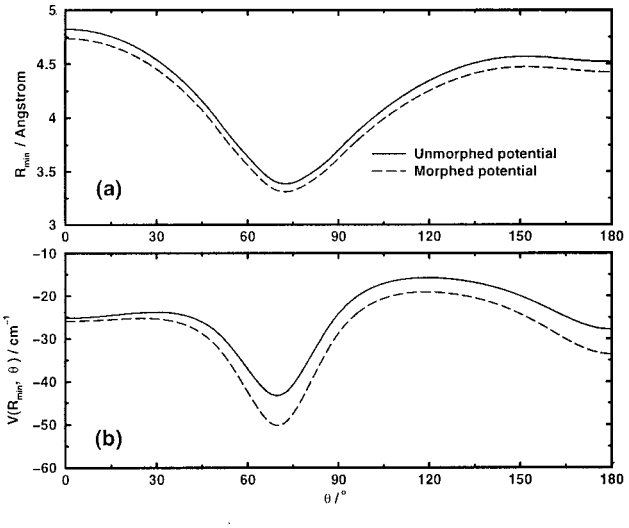

FIG. 4. Unmorphed (solid) and morphed (dashed) potentials for He–OCS. Lower graph, the minimum energy pathway against θ; upper graph, the values of R along the minimum energy pathway.

A contour plot of the anisotropically morphed potential is given in the bottom panel of Fig. 2. From the morphing parameters alone, given in Table II, it can be seen that morphing has made the potential approximately 16% deeper in the region of the global minimum, 3% deeper at the oxygen end, and 21% deeper at the sulfur end. Globally, ξ has been decreased by approximately 2%.

B. Comparison of the morphed and unmorphed potentials

The general shape of the potential has been retained following the morphing procedure, as can be seen by comparison of the unmorphed and morphed potentials in Fig. 2. This is a fundamental feature of the procedure. The effects can be seen more clearly in Fig. 4, which shows the distance of the minimum $R_m(\theta)$ and the corresponding well depth for the unmorphed and anisotropically morphed potentials as a function of θ. After morphing, the potential has become globally deeper, especially at the sulfur end.

The positions and energies of the stationary points of the anisotropically morphed potential and the unmorphed potential are compared in Table IV. The greatest amount of morphing was required at the sulfur end, where the morphed potential is made 5.76 cm^{-1} deeper and the distance of the minimum is reduced by 0.09 Å compared to the unmorphed potential. The global minimum is made 6.95 cm^{-1} deeper with a reduction in the equilibrium distance of 0.08 Å. The smallest adjustment is required at the oxygen end, with the morphed potential just 0.77 cm^{-1} deeper than the unmorphed potential and the minimum 0.09 Å closer in. The transition state closest to the oxygen end was made 1.43 cm^{-1} deeper, so that morphing has made the potential flatter at the oxygen end.

TABLE IV. Comparison of the energy and position of the stationary points of different He–OCS potentials. For the scaled HK potential, the energies are 10% larger and the positions of the stationary points are unchanged. Energies are given in cm^{-1} and positions are given in parentheses as (R/Å, θ/°). TS indicates a transition state and GM the global minimum.

Feature	Unmorphed	Anisotropic morphed	Unscaled HK (Ref. 13)
ϵ(O end)	−25.21(4.83,0.0)	−25.98(4.74,0.0)	−26.33(4.83,0.0)
ϵ(TS)	−23.84(4.55,29.5)	−25.28(4.54,25.1)	−24.46(4.51,32.2)
ϵ(GM)	−43.27(3.40,69.8)	−50.22(3.32,70.0)	−45.39(3.38,71.6)
ϵ(TS)	−15.81(4.33,119.1)	−19.17(4.24,118.9)	−16.29(4.36,121.3)
ϵ(S end)	−27.90(4.52,180.0)	−33.66(4.43,180.0)	−28.69(4.53,180.0)

Since sulfur is larger than carbon and oxygen, it is more difficult to describe in *ab initio* calculations. In addition, sulfur has many more core electrons, and is likely to be more susceptible to the frozen core approximation made in our CCSD(T) calculations. It is therefore perhaps not surprising that the greatest deficiencies in the unmorphed potential are at the sulfur end.

C. Comparison of the HK and morphed surfaces

The unscaled HK surface is slightly deeper that our unmorphed potential at all angles, as shown in Table IV. The scaling introduced by Higgins and Klemperer was a simple 10% increase in the well depth at all geometries, so that the geometries of the stationary points are unaffected. However, their scaled potential is significantly deeper than our anisotropically morphed potential at the oxygen end, but shallower at the sulfur end. It may be noted that Higgins and Klemperer also kept the core electrons frozen in their *ab initio* calculations, as we did.

The calculated transition frequencies reported by Higgins and Klemperer[13] for the unscaled HK potential are included in Table III. It may be seen that our unmorphed potential agrees more closely with six of the ten rotational transitions than the HK potential. Comparisons are made with the unscaled HK potential because only effective Hamiltonian parameters and not raw transition frequencies for the scaled HK potential were reported in Ref. 13.

The greatest difference between the observed and calculated transitions for the unscaled HK potential is in the $2_{21} \leftarrow 1_{10}$ transition where the difference is 1316.8 MHz. Our unmorphed potential is slightly better, with a difference of 1039.9 MHz for the same transition. The isotropically morphed potential gives a marked improvement, with the greatest difference being 239.6 MHz, for the $2_{11} \leftarrow 1_{10}$ transition. For the anisotropically morphed potential, there are no differences greater than 1.0 MHz.

Higgins and Klemperer showed that scaling the MP4 potential led to improved agreement with the rotational constants and their (differently defined) centrifugal distortion constants. However, even with this scaling, the agreement is not nearly as close as with the anisotropically morphed potential.

All the states that were observed by Higgins and Klemperer were rotational states of the ground vibrational state. As they showed, this state is quite strongly angularly localized, with most of its probability density between $\theta = 50°$ and 90°. However, the first two excited states sample quite different regions of space.[13] It is therefore interesting to compare the energies of the excited states, and this is done in Table V. Our best estimate of the ground state energy, from the anisotropically morphed potential, is $-18.6\ cm^{-1}$; this may be compared with $-19.1\ cm^{-1}$ for the scaled HK potential, which also has one more bound state than the unscaled HK potential or either of the morphed potentials. It may be seen that the frequencies of transitions to the excited intermolecular vibrations are indeed significantly different for the three potentials, so measurements of these frequencies would be a good way to distinguish between them.

TABLE V. Calculated bound states energies of He–OCS for $J=0$ (in cm^{-1}).

Energy level	Isotropic morphed	Anisotropic morphed	Scaled HK (Ref. 13)
1	−22.713	−18.625	−19.112
2	−12.867	−10.275	−10.337
3	−11.856	−9.194	−9.250
4	−9.129	−6.526	−6.826
5	−6.665	−4.102	−4.576
6	−3.682	−1.598	−1.611
7			−0.181

VI. CONCLUSIONS

The morphing procedure has been successfully applied to the potential energy surface of He–OCS. The unmorphed potential has closer agreement with the majority of experimentally observed transitions than the HK surface, so it appears that the grid of points used for the *ab initio* computations was appropriate. The amount of morphing required was small compared to previously published applications of morphing[19,37] because of the high quality of the initial surface. Our recommended potential, the anisotropically morphed potential, reproduces the measured rotational transitions to within 1 MHz.

The remaining uncertainties in the He–OCS potential are principally in the balance between the depths of the subsidiary wells at the two ends of the OCS molecule. The most useful further experiments to resolve the uncertainties would be measurements of transitions involving excited intermolecular vibrations, which sample more of the angular space than the pure rotational transitions included in the present fit.

VII. ADDITIONAL MATERIAL

A FORTRAN77 subroutine and data file are available to evaluate the He–OCS morphed potential. These can be obtained via anonymous ftp from krypton.dur.ac.uk.

[1] J. P. Toennies and A. F. Vilesov, Annu. Rev. Phys. Chem. **49**, 1 (1998).
[2] M. Hartmann, N. Pörtner, B. Sartakov, J. P. Toennies, and A. F. Vilesov, J. Chem. Phys. **110**, 5109 (1999).
[3] S. Grebenev, J. P. Toennies, and A. F. Vilesov, Science **279**, 2083 (1998).
[4] A. Lindinger, J. P. Toennies, and A. F. Vilesov, J. Chem. Phys. **110**, 1429 (1999).
[5] J. Higgins, C. Callegari, J. Reho, F. Stienkemeier, W. E. Ernst, K. K. Lehmann, M. Gutowski, and G. Scoles, Science **273**, 629 (1996).
[6] K. Nauta and R. E. Miller, Science **283**, 1895 (1999).
[7] E. Lugovoj, J. P. Toennies, and A. Vilesov, J. Chem. Phys. **112**, 8217 (2000).
[8] S. Grebenev, M. Hartmann, M. Havenith, B. Sartakov, J. P. Toennies, and A. F. Vilsov, J. Chem. Phys. **112**, 4485 (2000).
[9] K. Nauta and R. E. Miller, J. Chem. Phys. **111**, 3426 (1999).
[10] K. Nauta and R. E. Miller, Phys. Rev. Lett. **82**, 4480 (1999).
[11] E. Lee, D. Farrelly, and K. B. Whaley, Phys. Rev. Lett. **83**, 3812 (1999).
[12] C. Callegari, A. Conjusteau, I. Reinhard, K. K. Lehmann, G. Scoles, and F. Dalfovo, Phys. Rev. Lett. **83**, 5058 (1999).
[13] K. Higgins and W. Klemperer, J. Chem. Phys. **110**, 1383 (1999).
[14] P. J. Dunlop and C. M. Bignell, Ber. Bunsenges. Phys. Chem. **99**, 77 (1995).
[15] M. Broquier, A. Picard-Berselini, B. J. Whitaker, and S. Green, J. Chem. Phys. **84**, 2104 (1986).
[16] L. J. Danielson, K. M. Mcleod, and M. Keil, J. Chem. Phys. **87**, 239 (1987).
[17] M. Keil, L. J. Rawluk, and T. W. Dingle, J. Chem. Phys. **96**, 6621 (1992).
[18] J. Sadlej and W. D. Edwards, Int. J. Quantum Chem. **46**, 623 (1993).
[19] M. Meuwly and J. M. Hutson, J. Chem. Phys. **110**, 8338 (1999).
[20] J. M. Bowman and B. Gazdy, J. Chem. Phys. **94**, 816 (1991).
[21] B. Gazdy and J. M. Bowman, J. Chem. Phys. **95**, 6309 (1991).
[22] J. M. Bowman and B. Gazdy, Chem. Phys. Lett. **200**, 311 (1992).
[23] J. M. Bowman and J. Qi, in *Fashioning a Model: Optimization Methods in Chemical Physics*, edited by A. Ernesti, J. M. Hutson, and N. J. Wright (CCP6, Daresbury, 1998), p. 24.
[24] J. M. M. Howson and J. M. Hutson (unpublished).
[25] D. E. Woon and T. H. Dunning, Jr., J. Chem. Phys. **100**, 2975 (1994).
[26] T. H. Dunning, Jr., J. Chem. Phys. **90**, 1007 (1989).
[27] D. E. Woon and T. H. Dunning, Jr., J. Chem. Phys. **98**, 1358 (1993).
[28] Basis sets were obtained from the Extensible Computational Chemistry Environment Basis Set Database, Version 1.0, as developed and distributed by the Molecular Science Computing Facility, Environmental and Molecular Sciences Laboratory which is part of the Pacific Northwest Laboratory, P.O. Box 999, Richland, Washington 99352, USA, and funded by the U.S. Department of Energy. The Pacific Northwest Laboratory is a multi-program laboratory operated by Battelle Memorial Institue for the U.S. Department of Energy under Contract No. DE-AC06-76RLO 1830. Contact David Feller or Karen Schuchardt for further information.
[29] S. F. Boys and F. Bernardi, Mol. Phys. **19**, 553 (1970).
[30] M. J. Frisch, G. W. Trucks, H. B. Schlegel *et al.*, GAUSSIAN 94, Revision C.3, Gaussian, Inc., Pittsburgh, PA, 1995.
[31] T.-S. Ho and H. Rabitz, J. Chem. Phys. **104**, 2584 (1996).
[32] J. M. Hutson, Comput. Phys. Commun. **84**, 1 (1994).
[33] J. M. Hutson, BOUND computer program, version 6, distributed by Collaborative Computational Project No.6 of the UK Science and Engineering Research Council, 1993.
[34] E. Rbaihi, A. Belafhal, J. V. Auwera, S. Naim, and A. Fayt, J. Mol. Spectrosc. **191**, 32 (1998).
[35] M. M. Law and J. M. Hutson, Comput. Phys. Commun. **102**, 252 (1997).
[36] M. M. Law and J. M. Hutson, I-NoLLS computer program version 1.0, 1996.
[37] M. Meuwly, J. Chem. Phys. **111**, 2633 (1999).